Volume 24
Number 35
21 September 2022
Pages 20569–21496

PCCP

Physical Chemistry Chemical Physics

rsc.li/pccp

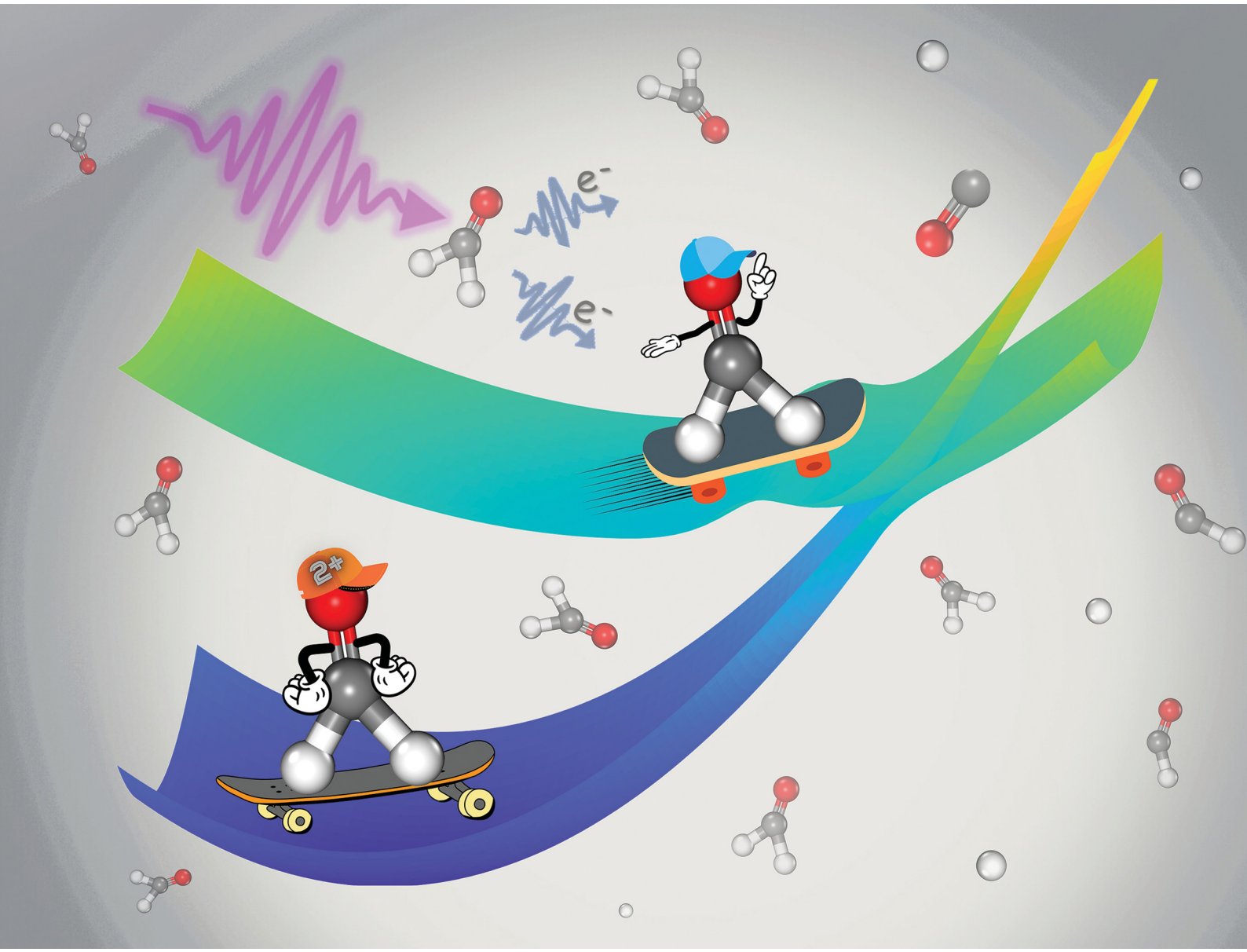

ISSN 1463-9076

ROYAL SOCIETY OF CHEMISTRY

PAPER

Spiridoula Matsika *et al.*

Stable excited dication: trapping on the S_1 state of formaldehyde dication after strong field ionization

PCCP

PAPER

View Article Online
View Journal | View Issue

Cite this: *Phys. Chem. Chem. Phys.*, 2022, **24**, 20701

Stable excited dication: trapping on the S_1 state of formaldehyde dication after strong field ionization†

Vaibhav Singh,[a] Chuan Cheng,[b] Thomas Weinacht[b] and Spiridoula Matsika *[a]

Received 9th June 2022,
Accepted 20th July 2022

DOI: 10.1039/d2cp02604j

rsc.li/pccp

Combined theoretical and experimental work examines the dynamics of dication formaldehyde produced by strong field ionization. Trajectory surface hopping dynamics on the first several singlet electronic states of the formaldehyde dication are used to examine the relaxation pathways and dissociation channels, while kinetic energy distributions after strong field ionization of formaldehyde and deuterated formaldehyde are used to confirm the theoretical predictions. We find that the first excited state of the formaldehyde dication is stable, neither decays to the ground state nor dissociates, even though the ground state and higher lying states are directly dissociative. The stability of the first excited state is explained by its symmetry which does not allow for radiative or nonradiative transitions to the ground state and by large barriers to dissociate on the excited state surface.

1 Introduction

Excited state dynamics in closed shell, neutral organic molecules drive organic photochemistry, and thus have been studied extensively.[1,2] When excitation occurs on higher excited states, Kasha's rule[3] is expected to be followed, *i.e.* relaxation to the lowest excited state occurs rapidly while a slower decay (radiative or radiationless) occurs from the first excited state, S_1, to the ground state. This is because the energetic gap between the closed shell ground state and the first excited state is usually large, while the gap between excited states is much smaller. So, a cascade of nonadiabatic transitions can easily relax the excited population to the S_1 state. In radical cations, however, the situation is different, since it is more likely that the spacing between the ground and first excited state is comparable to the gap between excited states. So, in that case rapid radiationless relaxation to the ground state is expected, and it is often observed.[4–8] Dications should be similar to monocations where the density of electronic states is high. There is however the possibility that the ground state of the dication is also closed shell if both electrons are ejected from the same orbital. In that case, the gap between the ground state and excited state may be larger than what one would intuitively expect.[9,10] Nevertheless, the gaps are still smaller than for neutral molecules, and a long-lived excited state is not intuitively expected.

In general, multiply charged cations in their excited state created by ionization are usually unstable, and they dissociate fast to create various fragments.[11–13] In most cases the fragmentation process occurs very fast, although there have been cases where delayed fragmentation from excited dications after ionization has been observed. In ethylene and acetylene, for example, dications with lifetimes ranging from hundreds of nanoseconds to microseconds were observed.[14] The delayed fragmentation process in ethylene is believed to occur on the electronically excited state, while in acetylene it occurs after intersystem crossing to the ground state.[14] Another example of long-lived excited state in dications has been observed in CO_2^{2+}, where the singly excited state is bound while the ground state is dissociative.[15,16] Metastable excited states have also been found in the diatomic dication Ne_2^{2+} leading to excimers. The first clear evidence for the existence of metastable Ne_2^{2+} has been established by Ben-Itzhak *et al.*[17] It was shown later that while the ground state is unstable, excited states are responsible for the observed dication.[18]

Metastable molecules in their excited states can be important intermediates where the stored electronic energy can be used to facilitate other reactions.[10,19] For example, in atmospheric chemistry or intergalactic chemistry, the long lifetime of excited metastable states enables the initiation of reactions through collision with other species.[20] Metastable excited states can also be used for population inversion, which is important for lasing. For this reason, the presence of long-lived excited states in charged ions is an important observation that should be studied in detail.

[a] *Department of Chemistry, Temple University, Philadelphia, PA 19122, USA. E-mail: smatsika@temple.edu*
[b] *Department of Physics, Stony Brook University, Stony Brook, NY 11790, USA*

† Electronic supplementary information (ESI) available: Additional information on dynamics results and excited state benchmarking. See DOI: https://doi.org/10.1039/d2cp02604j

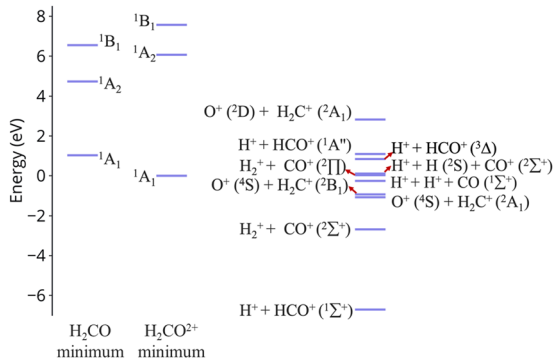

Fig. 1 Excitation energies of CH_2O^{2+} and dissociation energies of the fragments which are possible. Results are obtained at the CCSD/cc-pVQZ level of theory. Excitation energies are shown at two geometries, the minimum of neutral formaldehyde (corresponding to vertical ionization) and the minimum of the ground state of the dication. These geometries are shown in Fig. S1 (ESI†).

In this work we examine relaxation and fragmentation pathways in formaldehyde dication formed by strong field ionization. Based on the dissociation limits shown in Fig. 1 most dissociation channels are highly exothermic, and it is expected that dissociation will occur very fast. Theoretical calculations however show that dissociation from the first excited state is rare, and this is verified by experimentally observing the dication. Furthermore, the first excited state is predicted to be stable from relaxation to the ground state, having a much longer lifetime than what would be conventionally expected. We show that this surprising stability of the first excited state is due to the existence of barriers on the excited state preventing direct dissociation, and symmetry, which prohibits decay to the ground state.

2 Methods

2.1 Computational methods

The geometries of formaldehyde and its dication were optimized using the B3LYP[21–24] functional of Density Functional Theory[25,26] and the cc-pV5Z[27] basis set. The appearance energies of the fragments that could be formed possibly from dissociation of CH_2O^{2+} were calculated using coupled cluster singles and doubles (CCSD)[28] with the cc-pVQZ[27] basis set. The appearance energies of HCO^+, H_2C^+ in their first excited states were calculated using equation of motion-for excited energies-CCSD (EOM-EE-CCSD) with cc-pVQZ, whereas, the excited states of CO^+ were calculated using EOM- for ionization potential- CCSD (EOM-IP-CCSD) with cc-pVQZ starting from neutral CO.

In order to obtain potential energy surfaces along the C═O stretch, the single C–H (asymmetric C–H) stretch and the double C–H (symmetric C–H) stretch of CH_2O^{2+}, energies of the ground and excited states were plotted at the geometries produced with scans along each internal coordinate starting from the geometry of the neutral minimum of formaldehyde and stretching the corresponding bonds, while all the other degrees of freedom remain frozen at their initial value. The scans along asymmetric C–H were done using a state average of 10 states complete active space self consistent field with an active space of 8 electrons in 9 orbitals (10SA-CASSCF(8,9)) and the cc-pVDZ basis set. The scans along symmetric C–H and C═O were done at the CASSCF(8,9)/cc-pVDZ level of theory averaged over 4 A_1, 2 B_1, 2 B_2 and 2 A_2 states. Constrained optimizations along one C–H bond optimizing the S_1 state were done using a two-state average CASSCF (2SA-CASSCF(8,9)), since the optimizations were not converging when more states were included in the average, and a two-state average will give better description of S_1. The CASSCF(8,9)/cc-pVDZ calculations using the various averaging schemes were benchmarked by comparison to EOM-EE-CCSD with two larger basis sets, cc-pVTZ and cc-pVQZ. The energies are shown in ESI,† Tables S1 and S2, and confirm that this CASSCF approach is reasonable.

The B3LYP optimizations of formaldehyde geometries were done using the Gaussian09[29] suite of packages. All CCSD calculations were done with the Q-Chem[30] suite of packages. The CASSCF calculations were performed using COLUMBUS.[31–33]

Electronic state-resolved fragmentation of CH_2O^{2+} and the kinetic energy releases (KERs) for the different products are calculated with the help of the semi-classical molecular dynamics approach, trajectory surface hopping (TSH).[34,35] 200 initial conditions were generated using the harmonic oscillator Wigner distribution of the S_0 minimum of neutral CH_2O, with frequencies at the B3LYP/cc-pV5Z level of theory. The Wigner distribution code implemented in Newton-X[36] was used. The evolution of the classical trajectories was then studied separately for 6 singlet states of the dication, in order to get the dynamics and dissociation assuming ionization to each one of these states. The gradients along which the trajectories evolved, their electronic energies and non-adiabatic couplings at each time step, were calculated on-the-fly, with the help of quantum principles by applying 6SA-CASSCF(8,9)/cc-pVDZ level of theory. However, the nuclear motions were treated classically by applying the velocity-Verlet algorithm with a time step of 0.5 fs. The hopping probabilities between non-adiabatic states were dealt with the 'Fewest Switches Surface Hopping (FSSH)' algorithm,[37] as implemented in Newton-X.[38] The re-scaling of momentum after a hop was done along the derivative coupling vector in order to conserve the total energy. To deal with frustrated hops, *i.e.* when a trajectory does not have enough energy for a hop to occur, the momentum was left unaltered along the direction it was already moving. The decoherence correction of Persico and Grannuci[39] was used with a factor of 0.1 Hartree.[40]

70 of the 200 trajectories for each state were ran for 400 fs, but since the dynamics are practically done by 100 fs, the remaining 130 trajectories were run for 135 fs only. Many trajectories fail by the time they reach 100 fs. The number of trajectories that survived after 100 fs are 29, 28, and 35, for S_0, S_1 and S_2, respectively, while the numbers for S_3, S_4 and S_5 are even less, 14, 5, and 1 trajectories, respectively. This small number of trajectories complicates the statistics when calculating the population on each state, so we only show those up to 100 fs.

2.2 Experimental methods

The experimental setup has been described in detail in previous work.[41,42] Briefly, the output from a commercial amplified Ti:sapphire laser system (KM Labs, 1 mJ, 780 nm, 1 kHz, 30 fs) is sent into the vacuum chamber and is focused by a concave spherical silver mirror (f = 5 cm) to peak intensities between 40 and 240 TW cm^{-2} inside a Velocity Map Imaging (VMI) spectrometer. The VMI has a switchable three plate electrostatic lens stack, Microchannel Plates (MCP), phosphor screen, and camera (Tpx3Cam). The 1 ns resolution of the Tpx3Cam can resolve the 3D-vector momenta of ions, or 2-D electron momenta projected on the plane of the detector. The focused laser intensity is calibrated using the VMI to measure the classical $2U_p$ cut-off for electrons arising from strong field ionization of argon.[43]

The vacuum system consists of source and spectrometer chambers. The sample, deuterated formaldehyde, obtained by sublimation of paraformaldehyde-d2 (purity 98%, Sigma-Aldrich), is heated to 50–60 °C. A skimmed molecular beam of the target D_2O molecules intersects the laser in the interaction region of the VMI.[41] The deuterated version of the molecule is chosen to avoid potential contamination with low mass atomic ions like H^+.

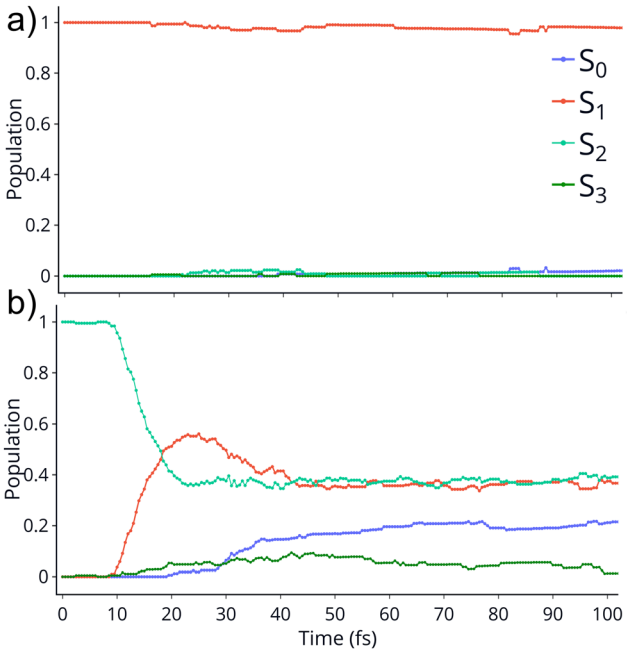

Fig. 2 Populations of 4 singlet states vs time for the trajectories initiated at S_1 (top) and S_2 (bottom). The populations on S_4 and S_5 are not shown since they remain zero for the whole dynamics.

3 Results and discussion

3.1 Dynamics on the S_1 surface

TSH dynamics were run starting from the ground and first five singlet excited states of the dication. Results of how the populations evolve in time for states S_1 and S_2 are shown in Fig. 2 while populations for the remaining states are shown in ESI.† When the dynamics are initiated on the S_1 state, the population remains on that state for more than 100 fs. After 150 fs only one trajectory has decayed to the ground state. So, there are practically no nonadiabatic transitions occurring. When the population is initially on the S_2 and higher states, population decays to lower states, as one would expect. Fig. 2 shows the populations for S_2 where decay to S_1 and eventually S_0 occurs rapidly. After 100 fs about 60% of the population has decayed to the lower states, with 40% being on S_1 and about 20% on the ground state. This pattern is similar for the other states.

An additional interesting observation when initiating dynamics on S_1 is that most of the trajectories show no dissociation. Only 16/200 trajectories fragment to CHO^+ and H^+ (see Table S3 in ESI†). On the other hand, half of the trajectories on S_2 dissociate to a three body channel $CO^+ + H^+ + H$. Plots of internal coordinates as a function of time in Fig. 3 show the dissociation patterns for the two states. Trajectories on the S_1 surface do not show any breaking of the C–O bond, while there is a small number of trajectories that break the C–H bonds. On the contrary, trajectories on the S_2 surface show a very fast dissociation along the C–H bonds. As shown in Fig. 3 C–H dissociation occurs within the first period of their oscillation, and the majority is symmetric. According to Fig. 1 all dissociation channels are exothermic with respect to the S_2 surface, and five of them are exothermic when exciting to the S_1 surface. Given the results of the dynamics, it is obvious that exothermicity alone cannot predict the dissociation patterns. In the case of S_1 specifically, it is intriguing that despite so many channels being energetically accessible minimal dissociation is observed. A more detailed investigation into what determines the dynamics is needed.

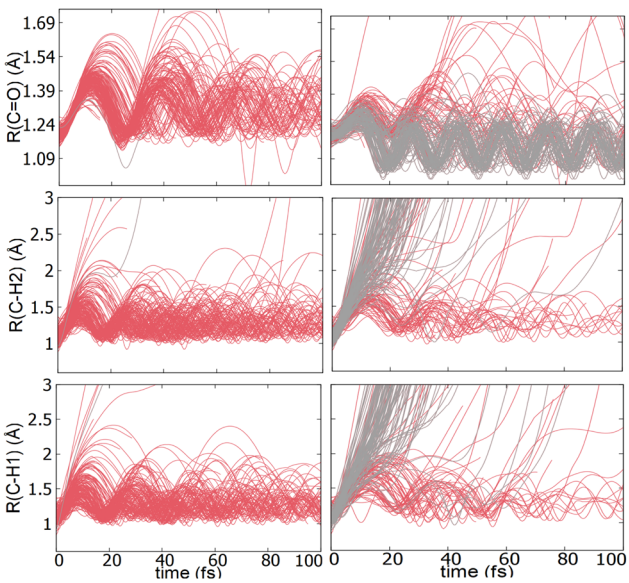

Fig. 3 Plots of internal coordinates *vs.* time for the dynamics ran on the S_1 (left) and S_2 (right) states. The trajectories dissociating to 3 fragments such as $CO + H^+ + H^+$ and $CO^+ + H^+ + H$ are shown in grey.

3.2 Symmetry prevents nonadiabatic transitions from S_1 to S_0

Many of the observations seen in the TSH calculations can be explained by symmetry. Formaldehyde and its dication have C_{2v} symmetry at their equilibrium geometries, and the electronic states belong to the corresponding irreducible representations. Fig. S9 in ESI† shows the configurations for the electronic states. The ground state of the dication is created by removing two electrons from the $2b_1$ orbital leading to a closed shell configuration with A_1 symmetry. The S_1 state is created by exciting an electron from $1b_2 \rightarrow 2b_1$, leading to an A_2 symmetry. S_2 is created by an excitation $5a_1 \rightarrow 2b_1$, leading to B_1 overall symmetry, while the symmetries of the other states at vertical ionization are A_1, B_1, A_1 for S_3, S_4, and S_5, respectively.

A_2 has unique properties compared to the other irreducible representations in C_{2v} symmetry. Since the symmetries of S_1 and S_0 are A_2 and A_1, respectively, the nonadiabatic coupling between them should have a_2 symmetry, which means that an a_2 vibration is needed to couple the two. But an a_2 vibration does not exist in formaldehyde. So, there is no nuclear motion that can lead to a coupling between the two states while C_{2v} symmetry is preserved. This has profound consequences, as we see in the dynamics. Furthermore, the radiative transitions between A_2 and the A_1 ground state are also forbidden by symmetry. This creates the conditions for a trapped state, both radiatively and nonradiatively.

Fig. 4 show the dissociation pathways in formaldehyde dication that retain C_{2v} symmetry. These are either C═O breaking or C–H symmetric stretch. Along C═O stretching, S_1 and S_0 actually become degenerate at large nuclear separations. If the degeneracy could facilitate nonadiabatic transitions, then the S_1 population could transfer to S_0 and possibly lead to further dissociation along other coordinates. But no such hoppings are observed due to symmetry! Along the C–H symmetric stretch the S_1 state crosses S_2 and S_3 and is diabatically correlated with an excited channel leading to $CO(^2\Pi) + H + H^+$. Again there are no transitions with any other state.

Finally, along the C–H asymmetric stretch coupling with the ground state could occur because the C_{2v} symmetry is broken. However S_1 remains more than 5 eV separated from S_0 everywhere along the path, so again the coupling will be very small, because of the energy gap this time.

There is the possibility however that geometries deviating from these rigid scans can be accessed, where for example the C–O bond is stretched while at the same time symmetry is broken by asymmetric stretch of the C–H bonds. This motion however does not seem important in the dynamics. By examining the trajectories we see that when the C–O bond is stretched the asymmetry between the two C–H bonds remains very small, so even when the molecule does not have strictly C_{2v} symmetry, it remains close to that symmetry and the nonadiabatic coupling remains small. More details of this analysis can be found in ESI† (Fig. S10).

3.3 No fragmentation on excited state surface

Although no transitions to the ground state occur, fragmentation could proceed along the excited state surface without need for decay to the ground state. However, Fig. 4 shows that the barriers for dissociation on the S_1 surface are very high (more than 2 eV) along C–O and symmetric C–H. The barrier along the asymmetric C–H breaking as shown in Fig. 4(c) is lower, so there is some possibility to break one C–H bond to produce the $H^+ + HCO^+$ in its excited state. Since the paths in this figure are

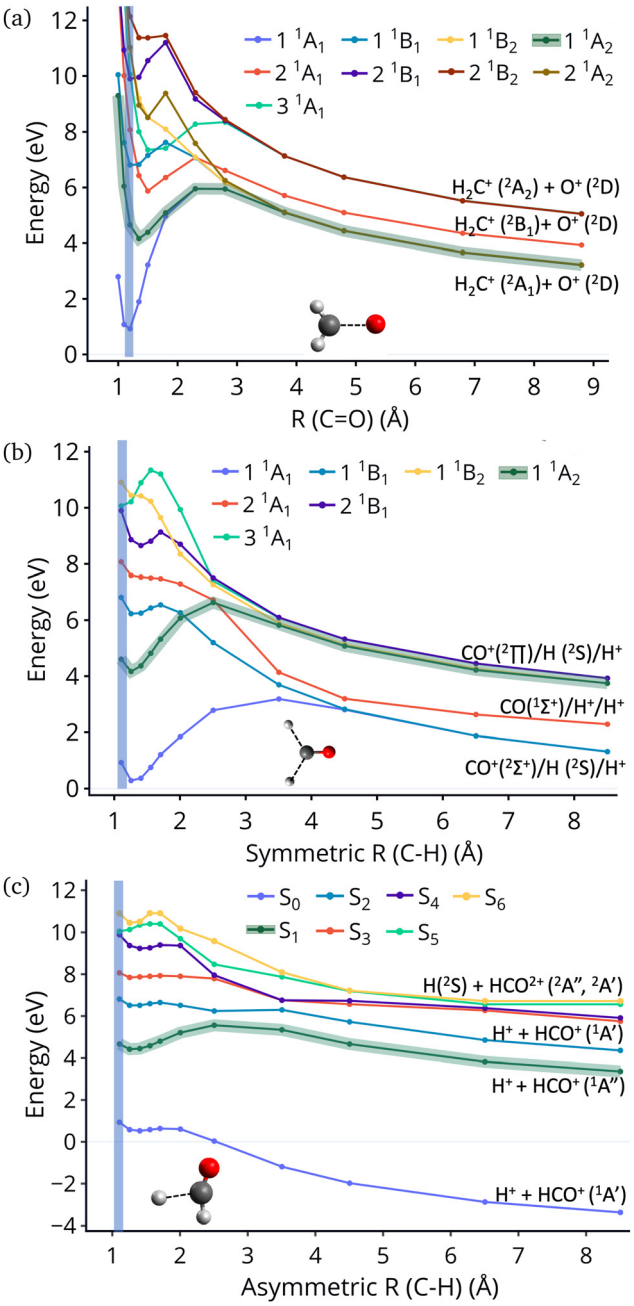

Fig. 4 Energies of singlets calculated at the geometries produced along C═O stretch (a); symmetric C–H stretch with both bonds being stretched (b); asymmetric C–H stretch where only one CH is stretched (c). The calculations were done at the CASSCF(8,9)/cc-pVDZ level of theory. The region of vertical excitation is highlighted with blue vertical line. The curve representing the S_1 state is highlighted with green thick line. In panels (a and b) that use symmetry this is the 1^1A_2 state, while for panel (c) it is the first excited S_1 across the whole curve.

based on rigid scans, the barriers are upper bounds to true barriers. In order to have a better estimate of the actual barrier along the asymmetric C–H path we performed constrained optimizations with one C–H bond constrained, while the other degrees of freedom were optimized. This path is shown in ESI† (Fig. S2), and leads to a barrier along the C–H bond of 0.8 eV. This explains why the only products seen for 16 out of 200 trajectories are along this pathway and lead to $HCO^+ + H^+$.

The non-dissociating trajectories on S_1 show some coherent oscillations along all 3 coordinates as shown in Fig. 3, although the C–O vibrations lose coherence rapidly after a few oscillations due to coupling between modes.

The dissociation of CH_2O^{2+} on the ground state surface forms HCO^+ ($^1\Sigma^+$) with linear geometry and H^+. However, the geometry of HCO^+ on its S_1 minimum is not linear with the H–C–O angle of 125°. The same has been seen by Weis and Yamashita.[44] Hence, when dissociation occurs on the first excited state it will lead to a nonlinear HCO^+ with a symmetry of $^1A''$ instead of $^1\Sigma^-$. Similarly, the degenerate second and third excited states of HCO^+ ($^1\Delta$ in linear symmetry) split into $^1A'$ and $^1A''$ states at the nonlinear S_1 minimum. This further suggests that the produced HCO^+ will be vibrationally excited along the bending mode.

3.4 Dynamics on the other singlet states

It is interesting to contrast the dynamics occurring on the S_1 surface with that of the S_2 and higher states. Fig. 2 shows that when the population is initially on the S_2 electronically excited state there is substantial decay to S_1 and S_0 within 100 fs. Specifically, about 40% of the population remains on S_2 while 40% decays to S_1 and 20% has reached the ground state after 100 fs. Fig. S8 in ESI† shows the populations for the other states. All the excited states lose more than 50% of their population within 20 fs. The statistics are not reliable for the higher states beyond 50 fs so we cannot predict the final distribution, but it is clear that radiationless decay is very fast. It should also be noted that when exciting to higher states the population does not get trapped on S_1 but it decays further to the ground state, for the most part. This is because all these nonadiabatic transitions break the symmetry, so S_1 is not an A_2 state anymore.

There is also substantial fragmentation observed in the dynamics of higher states. Table S3 in ESI† shows all the fragmentation products for each state. When starting on the S_2 state most of the population dissociates *via* a three-body dissociation to produce $CO^+ + H + H^+$ or $CO + H^+ + H^+$, regardless of the state on which fragmentation occurs. This is obvious in Fig. 3 which shows that both of the CH bonds break symmetrically. Fig. 4b shows that S_2 is strongly exothermic along the symmetric CH stretch coordinate, so that explains why this is the preferred dissociation mechanism. The data indicate that even when there is a nonadiabatic transition from S_2 to S_1, diabatically the population remains on the B_1 surface. The B_1 state dissociates *via* three body dissociation, while the A_2 state is bound along that coordinate. Fig. 3 shows that the C═O continues to vibrate coherently (significantly longer than in S_1) after the loss of the hydrogens. We note that it is with a higher frequency, as one would expect since the bond is stronger for CO^+. The dominant channel for states S_3, S_4 and S_5 is dissociation along the C═O bond leading to $CH_2^+ + O^+$, with O^+ being produced on its excited ^2D state rather than the ground ^4S state because of spin restrictions.

Dynamics on the ground state also predict fast dissociation. Almost all of the trajectories that have not failed lead to $HCO^+ + H^+$, since this pathway is more than 6 eV exothermic with a very small barrier on the ground state. Overall, a very small number of trajectories have not dissociated after 100 fs when starting from any other state except S_1.

3.5 Experimental observation of CD_2O^{2+}

As a test of the theoretical predictions, we carried out measurements on CH_2O as well as CD_2O. Both measurements showed evidence for the parent dication (CH_2O^{2+} or CD_2O^{2+}) in the time of flight mass spectrum. However, the signal for CH_2O^{2+} suffered from contamination by high energy O^+ and CH_2^+ fragments, and for CD_2O^{2+} the signal was also complicated by the detection of O^+/CD_2^+ fragments, which have the same time of flight (TOF) due to their common mass over charge. In order to clarify the evidence for the formation of a stable dication, we carried out detailed momentum resolved measurements of the fragment ions, which allowed us to distinguish O^+ and CD_2^+ from CD_2O^{2+}.

Fig. 5 shows the angular distribution for the ions having TOF corresponding to these fragments with different laser intensities. The variation of the angular distribution with laser intensity reveals multiple contributions to the yield. At low intensities, one can see a clear variation in the yield with angle, which is consistent with O^+ and CD_2^+ fragments formed from dissociative single ionization. However, for higher laser intensities (bottom three panels of Fig. 5), the yield does not vary with angle, which is consistent with non-dissociative double ionization.

In strong field ionization, single ionization is generally dominant at low intensities. As the intensity increases, higher order ionization becomes more prominent.[42,45–49] Thus it makes sense that the $O^+/CD_2^+/CD_2O^{2+}$ signal for low intensities is dominated by fragments arising from dissociative single ionization, with Kinetic Energy Release (KER) between 0 and 1.3 eV, while the $O^+/CD_2^+/CD_2O^{2+}$ signal for high intensities is dominated by the dication formed by double ionization, with KER between 1 and 5 eV.

As further evidence for the formation of the stable dication, we consider the KER for fragment ions at the position of the parent dication in the TOFMS. The expectation is that the dication parent should show very low KER since there is no dissociation involved. The KER distribution as a function of laser intensity is shown in Fig. 6. For low intensities (0 to 75 TW cm^{-2}), dissociative single ionization dominates, producing relatively low energy O^+ or CD_2^+ fragments. As the intensity goes higher (75 to 150 TW cm^{-2}), the production of energetic fragments (2 to 5 eV) from dissociative single or double ionization dominates. Finally, for the highest intensities, we see very

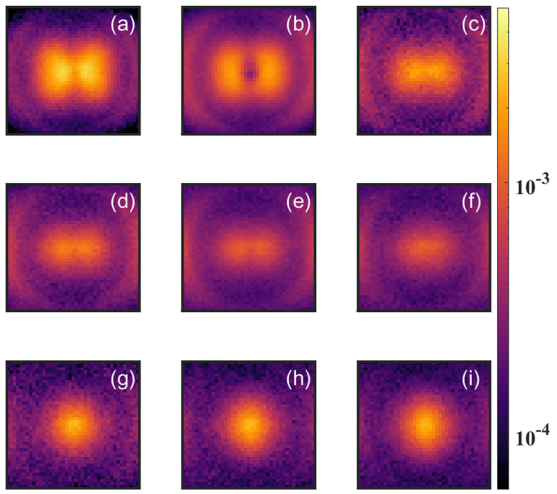

Fig. 5 Two dimensional projection of the momentum distribution for O^+ (CD_2O^{2+}) produced with various laser intensities. The laser polarization is along horizontal direction in all the panels. The momentum range of ±40 a.u. is displayed at each intensity. The subpanels are ordered with laser peak intensity at (a–i) 43, 67, 96, 120, 144, 168, 192, 216, 240 TW cm^{-2}, respectively. The low KE (center region) change its shape and relative amplitude dramatically as the intensity changes. This change in angular distribution indicates that at different intensity, the low KE O^+ (CD_2O^{2+}) are coming from different mechanism.

high energy fragments (greater than 5 eV) being formed, in addition to an increase in very low KER ions. The very high energy fragments can be associated with dissociative double and triple ionization, while the low energy fragments point to the formation of CD_2O^{2+}, which is consistent with the angular distributions at high intensity discussed above.

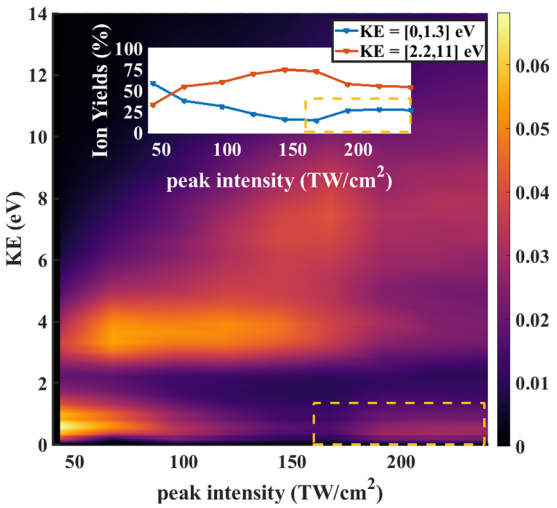

Fig. 6 KE distribution of O^+ (CD_2O^{++}) fragment as function of laser power (peak intensity). The single ionization's contribution is mostly at the low KE low intensity region (0 to 1.3 eV). The double ionization is thought to be higher KE higher intensity region (2.2 to 11 eV). The even higher ionization channels are showing in the even higher KE even higher intensity. And at really high intensity, low KE region, we see ion yields which are presumably from the non-dissociative double ionization CD_2O^{++}, which coincides at the same mass-to-charge ratio with the O^+ fragment.

We note that strong field ionization leads to the population of multiple states of the dication, not only S_1. However, given that the calculations indicate that only S_1 is stable, and that our measurements agree with the calculations quantitatively regarding the dissociation energies from other states of the dication,[50] we believe that our measurements of the dication come from molecules in the S_1 state of the dication.

4 Conclusions

In conclusion, we have shown that the first excited state of the formaldehyde dication is stable both from decay to the ground state and from dissociation, even though the ground state and higher lying states are directly dissociative. This is a rather unexpected result because in general double ionization of closed shell molecules creates rather unstable species. Furthermore, when these dications are electronically excited they are expected to be even more unstable because of all the extra available energy. A stable excited state when the ground state is dissociative is possible here because of the high symmetry of formaldehyde which restricts the types of vibrations that can couple the different states. One may imagine that other molecules with high symmetry can be found that show similar dynamics. A bound excited state combined with a dissociative ground state can be useful in laser action. Excimer lasers create population inversion because they have a bound excited state, but a dissociative ground state. Emission is not possible in the current system since the S_1 state has a zero transition dipole moment with the ground state by symmetry. The pair S_0 (A_1 symmetry)–S_1 (A_2 symmetry) in formaldehyde dication has both a zero radiative coupling (through the transition dipole moment operator) and radiationless coupling (through the nonadiabatic coupling operator). Since however these two operators are different a system that has zero nonadiabatic coupling but nonzero radiative coupling could create population inversion.

The calculations described here motivate the measurement of dynamics in the stable dication. The analysis of the trajectories in Fig. 3 shows coherent C–O oscillations in S_1, which could be detected by covariance pump probe measurements of the fragment ion yields. A pump pulse could launch a vibrational wave packet on the S_1 state of the dication, which could be probed *via* further ionization to the trication, followed by momentum resolved measurements of the fragment ions in covariance.[51]

Conflicts of interest

There are no conflicts to declare.

Acknowledgements

The authors gratefully acknowledge the Department of Energy (DOE, Award no. DE-FG02-08ER15983 for V. S. and S. M. and DOE, Award no. DE-FG02-08ER15984 for C. C. and T. W.) for

funding. Part of the computational work was performed using the Extreme Science and Engineering Discovery Environment (XSEDE), which is supported by National Science Foundation Grant no. ACI-1548562.

Notes and references

1 M. Klessinger and J. Michl, *Excited States and Photochemistry of Organic Molecules*, VCH Publishers, Inc., New York, 1995.
2 W. Domcke, D. R. Yarkony and H. Köppel, *Conical Intersections: Theory, Computation and Experiment*, World Scientific, Singapore, 2011.
3 M. Kasha, *Discuss. Faraday Soc.*, 1950, **9**, 14–19.
4 M. Assmann, T. Weinacht and S. Matsika, *J. Chem. Phys.*, 2016, **144**, 034301.
5 H. Koppel, M. Doscher, I. Baldea, H. Meyer and P. Szalay, *J. Chem. Phys.*, 2002, **117**, 2657–2671.
6 H. Tao, L. Shen, M. H. Kim, A. G. Suits and T. J. Martinez, *J. Chem. Phys.*, 2011, **134**, 054313.
7 B. Joalland, T. Mori, T. J. Martinez and A. G. Suits, *J. Phys. Chem. Lett.*, 2014, **5**, 1467–1471.
8 K. Munkerup, D. Romanov, T. Bohinski, A. B. Stephansen, R. J. Levis and T. I. Solling, *J. Phys. Chem. A*, 2017, **121**, 8642–8651.
9 A. Zhao, P. Sańdor, V. Tagliamonti, S. Matsika and T. Weinacht, *J. Phys. Chem. A*, 2016, **120**, 3233–3240.
10 S. Banhatti, J. Palotás, P. Jusko, B. Redlich, J. Oomens, S. Schlemmer and S. Brünken, *Astron. Astrophys.*, 2021, **648**, A61.
11 T. Osipov, T. N. Rescigno, T. Weber, S. Miyabe, T. Jahnke, A. S. Alnaser, M. P. Hertlein, O. Jagutzki, L. P. H. Schmidt, M. Schöffler, L. Foucar, S. Schössler, T. Havermeier, M. Odenweller, S. Voss, B. Feinberg, A. L. Landers, M. H. Prior, R. Dörner, C. L. Cocke and A. Belkacem, *J. Phys. B: At., Mol. Opt. Phys.*, 2008, **41**, 091001.
12 X. Zhou, P. Ranitovic, C. Hogle, J. H. D. Eland, H. C. Kapteyn and M. M. Murnane, *Nat. Phys.*, 2012, **8**, 232–237.
13 G. Basnayake, P. Hoerner, B. Mignolet, M. K. Lee, Y. F. Lin, A. H. Winney, D. A. Debrah, L. Popaj, X. Shi, S. K. Lee, H. B. Schlegel, F. Remacle and W. Li, *Phys. Chem. Chem. Phys.*, 2021, **23**, 23537–23543.
14 S. Larimian, S. Erattupuzha, E. Lotstedt, T. Szidarovszky, R. Maurer, S. Roither, M. Schoeffler, D. Kartashov, A. Baltuska, K. Yamanouchi, M. Kitzler and X. Xie, *Phys. Rev. A*, 2016, **93**, 053405.
15 M. Alagia, P. Candori, S. Falcinelli, M. Lavollée, F. Pirani, R. Richter, S. Stranges and F. Vecchiocattivi, *J. Phys. Chem. A*, 2009, **113**, 14755–14759.
16 S. Falcinelli, *Acta Phys. Pol.*, 2017, **131**, 112–116.
17 I. Ben-Itzhak, I. Gertner, D. Bortman and D. Zajfman, *Phys. Rev. A: At., Mol., Opt. Phys.*, 1990, **41**, 6548.
18 J. Ackermann and H. Hogreve, *Phys. Chem. Chem. Phys.*, 2017, **19**, 32433–32442.
19 P. Tosi, R. Correale, W. Lu, S. Falcinelli and D. Bassi, *Phys. Rev. Lett.*, 1999, **82**, 450–452.
20 M. Torr and D. Torr, *Rev. Geophys.*, 1982, **20**, 91–144.
21 A. D. Becke, *J. Chem. Phys.*, 1993, **98**, 5648–5652.
22 A. D. Becke, *Phys. Rev. A: At., Mol., Opt. Phys.*, 1988, **38**, 3098.
23 C. Lee, W. Yang and R. G. Parr, *Phys. Rev. B: Condens. Matter Mater. Phys.*, 1988, **37**, 785.
24 S. H. Vosko, L. Wilk and M. Nusair, *Can. J. Phys.*, 1980, **58**, 1200–1211.
25 T. Ziegler, *Chem. Rev.*, 1991, **91**, 651–667.
26 W. Kohn, A. D. Becke and R. G. Parr, *J. Phys. Chem. A*, 1996, **100**, 12974–12980.
27 T. H. Dunning, *J. Chem. Phys.*, 1989, **90**, 1007–1023.
28 G. D. Purvis III and R. J. Bartlett, *J. Chem. Phys.*, 1982, **76**, 1910–1918.
29 M. J. Frisch, G. W. Trucks, H. B. Schlegel, G. E. Scuseria, M. A. Robb, J. R. Cheeseman, G. Scalmani, G. A. P. V. Barone, H. Nakatsuji, X. Li, M. Caricato, J. B. A. Marenich, B. G. Janesko, B. M. R. Gomperts, H. P. Hratchian, J. V. Ortiz, A. F. Izmaylov, J. L. Sonnenberg, D. Williams-Young, F. Ding, F. Lipparini, F. Egidi, J. Goings, B. Peng, A. Petrone, T. Henderson, D. Ranasinghe, V. G. Zakrzewski, J. Gao, N. Rega, G. Zheng, W. Liang, M. Hada, M. Ehara, K. Toyota, R. Fukuda, J. Hasegawa, M. Ishida, T. Nakajima, Y. Honda, O. Kitao, H. Nakai, T. Vreven, K. Throssell, J. A. Montgomery, J. E. P. Jr., F. Ogliaro, M. Bearpark, J. J. Heyd, E. Brothers, K. N. Kudin, V. N. Staroverov, T. Keith, J. N. R. Kobayashi, K. Raghavachari, A. Rendell, J. C. Burant, S. S. Iyengar, J. Tomasi, M. Cossi, J. M. Millam, C. A. M. Klene, R. Cammi, J. W. Ochterski, R. L. Martin, K. Morokuma, O. Farkas, J. B. Foresman and D. J. Fox, *Gaussian 09, Revision A.02,* Gaussian, Inc., Wallingford CT, 2009.
30 Y. Shao, Z. Gan, E. Epifanovsky, A. T. Gilbert, M. Wormit, J. Kussmann, A. W. Lange, A. Behn, J. Deng, X. Feng, D. Ghosh, M. Goldey, P. R. Horn, L. D. Jacobson, I. Kaliman, R. Z. Khaliullin, T. Kuś, A. Landau, J. Liu, E. I. Proynov, Y. M. Rhee, R. M. Richard, M. A. Rohrdanz, R. P. Steele, E. J. Sundstrom, H. L. Woodcock III, P. M. Zimmerman, D. Zuev, B. Albrecht, E. Alguire, B. Austin, G. J. O. Beran, Y. A. Bernard, E. Berquist, K. Brandhorst, K. B. Bravaya, S. T. Brown, D. Casanova, C.-M. Chang, Y. Chen, S. H. Chien, K. D. Closser, D. L. Crittenden, M. Diedenhofen, R. A. DiStasio Jr., H. Dop, A. D. Dutoi, R. G. Edgar, S. Fatehi, L. Fusti-Molnar, A. Ghysels, A. Golubeva-Zadorozhnaya, J. Gomes, M. W. Hanson-Heine, P. H. Harbach, A. W. Hauser, E. G. Hohenstein, Z. C. Holden, T.-C. Jagau, H. Ji, B. Kaduk, K. Khistyaev, J. Kim, J. Kim, R. A. King, P. Klunzinger, D. Kosenkov, T. Kowalczyk, C. M. Krauter, K. U. Lao, A. D. Laurent, K. V. Lawler, S. V. Levchenko, C. Y. Lin, F. Liu, E. Livshits, R. C. Lochan, A. Luenser, P. Manohar, S. F. Manzer, S.-P. Mao, N. Mardirossian, A. V. Marenich, S. A. Maurer, N. J. Mayhall, E. Neuscamman, C. M. Oana, R. Olivares-Amaya, D. P. ONeill, J. A. Parkhill, T. M. Perrine, R. Peverati, A. Prociuk, D. R. Rehn, E. Rosta, N. J. Russ, S. M. Sharada, S. Sharma, D. W. Small, A. Sodt, T. Stein, D. Stück, Y.-C. Su, A. J. Thom, T. Tsuchimochi, V. Vanovschi, L. Vogt, O. Vydrov, T. Wang, M. A. Watson, J. Wenzel, A. White, C. F. Williams, J. Yang, S. Yeganeh, S. R. Yost, Z.-Q. You, I. Y. Zhang, X. Zhang, Y. Zhao,

B. R. Brooks, G. K. Chan, D. M. Chipman, C. J. Cramer, W. A. Goddard III, M. S. Gordon, W. J. Hehre, A. Klamt, H. F. Schaefer III, M. W. Schmidt, C. D. Sherrill, D. G. Truhlar, A. Warshel, X. Xu, A. Aspuru-Guzik, R. Baer, A. T. Bell, N. A. Besley, J.-D. Chai, A. Dreuw, B. D. Dunietz, T. R. Furlani, S. R. Gwaltney, C.-P. Hsu, Y. Jung, J. Kong, D. S. Lambrecht, W. Liang, C. Ochsenfeld, V. A. Rassolov, L. V. Slipchenko, J. E. Subotnik, T. V. Voorhis, J. M. Herbert, A. I. Krylov, P. M. Gill and M. Head-Gordon, *Molecular Physics*, 2015, **113**, 184–215.

31 H. Lischka, R. Shepard, R. M. Pitzer, I. Shavitt, M. Dallos, T. Müller, P. G. Szalay, M. Seth, G. S. Kedziora, S. Yabushita and Z. Zhang, *Phys. Chem. Chem. Phys.*, 2001, **3**, 664–673.

32 H. Lischka, R. Shepard, I. Shavitt, R. M. Pitzer, M. Dallos, T. Müller, P. G. Szalay, F. B. Brown, R. Ahlrichs, H. J. Böhm, A. Chang, D. C. Comeau, R. Gdanitz, H. Dachsel, C. Ehrhardt, M. Ernzerhof, P. Höchtl, S. Irle, G. Kedziora, T. Kovar, V. Parasuk, M. J. M. Pepper, P. Scharf, H. Schiffer, M. Schindler, M. Schüler, M. Seth, E. A. Stahlberg, J.-G. Zhao, S. Yabushita, Z. Zhang, M. Barbatti, S. Matsika, M. Schuurmann, D. R. Yarkony, S. R. Brozell, E. V. Beck, J.-P. Blaudeau, M. Ruckenbauer, B. Sellner, F. Plasser, J. J. Szymczak, R. F. K. Spada and A. Das, *COLUMBUS, an ab initio electronic structure program, release 7.0*, 2017.

33 H. Lischka, R. Shepard, T. Müller, P. G. Szalay, R. M. Pitzer, A. J. A. Aquino, M. M. Araújo do Nascimento, M. Barbatti, L. T. Belcher, J.-P. Blaudeau, I. Borges, S. R. Brozell, E. A. Carter, A. Das, G. Gidofalvi, L. González, W. L. Hase, G. Kedziora, M. Kertesz, F. Kossoski, F. B. C. Machado, S. Matsika, S. A. do Monte, D. Nachtigallová, R. Nieman, M. Oppel, C. A. Parish, F. Plasser, R. F. K. Spada, E. A. Stahlberg, E. Ventura, D. R. Yarkony and Z. Zhang, *J. Chem. Phys.*, 2020, **152**, 134110.

34 M. Barbatti, *Wiley Interdiscip. Rev.: Comput. Mol. Sci.*, 2011, **1**, 620–633.

35 J. C. Tully, *J. Chem. Phys.*, 2012, **137**, 22A301.

36 M. Barbatti, G. Granucci, M. Ruckenbauer, F. Plasser, R. Crespo-Otero, J. Pittner, M. Persico and H. Lischka, *NEWTON-X: a package for Newtonian dynamics close to the crossing seam, Version 2.2*, 2019.

37 J. C. Tully, *J. Chem. Phys.*, 1990, **93**, 1061–1071.

38 M. Barbatti, M. Ruckenbauer, F. Plasser, J. Pittner, G. Granucci, M. Persico and H. Lischka, *Wiley Interdiscip. Rev.: Comput. Mol. Sci.*, 2014, **4**, 26–33.

39 G. Granucci and M. Persico, *J. Chem. Phys.*, 2007, **126**, 134114.

40 C. Zhu, S. Nangia, A. W. Jasper and D. G. Truhlar, *J. Chem. Phys.*, 2004, **121**, 7658–7670.

41 A. Zhao, M. van Beuzekom, B. Bouwens, D. Byelov, I. Chakaberia, C. Cheng, E. Maddox, A. Nomerotski, P. Svihra and J. Visser, *et al.*, *Rev. Sci. Instrum.*, 2017, **88**, 113104.

42 C. Cheng, P. Vindel-Zandbergen, S. Matsika and T. Weinacht, *Phys. Rev. A*, 2019, **100**, 053405.

43 P. B. Corkum, *Phys. Rev. Lett.*, 1993, **71**, 1994.

44 B. Weis and K. Yamashita, *J. Chem. Phys.*, 1993, **99**, 9512–9520.

45 T. Zuo and A. D. Bandrauk, *Phys. Rev. A: At., Mol., Opt. Phys.*, 1995, **52**, R2511.

46 D. N. Fittinghoff, P. R. Bolton, B. Chang and K. C. Kulander, *Phys. Rev. Lett.*, 1992, **69**, 2642.

47 C. Guo, M. Li, J. P. Nibarger and G. N. Gibson, *Phys. Rev. A: At., Mol., Opt. Phys.*, 2000, **61**, 033413.

48 X.-M. Tong, Z. Zhao and C.-D. Lin, *Phys. Rev. A: At., Mol., Opt. Phys.*, 2002, **66**, 033402.

49 M. Kübel, C. Burger, N. G. Kling, T. Pischke, L. Beaufore, I. Ben-Itzhak, G. G. Paulus, J. Ullrich, T. Pfeifer and R. Moshammer, *et al.*, *Phys. Rev. A*, 2016, **93**, 053422.

50 C. Cheng, V. Singh, S. Matsika and T. Weinacht, submitted.

51 F. Allum, C. Cheng, A. J. Howard, P. H. Bucksbaum, M. Brouard, T. Weinacht and R. Forbes, *J. Phys. Chem. Lett.*, 2021, **12**, 8302–8308.

